

Spoiling of Transverse Magnetization in Gradient-Echo (GRE) Imaging during the Approach to Steady State

Frederick H. Epstein, John P. Mugler III, James R. Brookeman

The signal evolution behaviors and corresponding image appearances for different methods of spoiling or refocusing the transverse magnetization in short TR gradient-echo imaging during the approach to steady state were investigated experimentally and using computer simulations based on the Bloch equations. Specifically, ideally spoiled, gradient-spoiled, gradient-refocused, and RF-spoiled pulse sequence configurations were studied. This study showed that, for the gradient-spoiled configuration, the signal evolution is position and phase-encoding order-dependent and, under typical imaging conditions, can deviate substantially from the ideally spoiled signal evolution at some spatial positions, resulting in intensity banding image artifacts. For the gradient-refocused configuration, the signal evolution oscillates toward the steady state and, generally, does not closely approximate that of ideal spoiling, resulting in different image contrast or image blurring. Using RF spoiling, the signal evolution closely approximates the ideally spoiled case for flip angles less than approximately 20° and T_2 values of less than approximately 200 ms and results in relatively artifact-free images. Also, this study showed that, for RF spoiling, an RF-pulse phase-difference increment other than 117° , such as 84° , may be optimal for gradient-echo imaging during the approach to steady state.

Key words: rapid imaging; computer simulations; pulse sequences.

INTRODUCTION

Short repetition time (TR) gradient-echo (GRE) MRI techniques such as magnetization-prepared gradient echo (MP-GRE) and segmented GRE are finding a wide variety of applications including imaging the liver (1, 2), brain (3, 4), breast (4), spine (5), heart (6, 7), coronary arteries (8, 9), and renal arteries (10). Using TR values of approximately 10 ms or less and contrast preparation periods and/or relatively long inter-shot delay times, these sequences acquire image data while the measured signal evolves toward the steady state (11–13). These techniques differ from conventional GRE imaging [e.g., fast low angle shot (FLASH), gradient-recalled acquisition into steady state (GRASS), and fast imaging with steady

precession (FISP)] in which, using longer TR values and continuous (nonsegmented) data acquisition strategies, image data are acquired while the measured signal is in the steady state.

A major consideration in the design of pulse sequences for both conventional GRE imaging and GRE imaging during the approach to steady state is how to control residual coherent transverse magnetization (i.e., transverse magnetization generated by previous RF excitations, which is coherent just before current RF excitation). Two general approaches toward controlling residual coherent transverse magnetization have been taken. One approach is to eliminate, or “spoil,” this magnetization. Methods for spoiling magnetization include gradient spoiling (14–17) and RF spoiling (18, 19). Another approach is to preserve, or “refocus,” residual coherent transverse magnetization (20–23). Refocusing of the transverse magnetization is accomplished by applying a compensatory gradient pulse on the phase-encode axis, equal in amplitude and opposite in polarity to the phase-encoding gradient, after the data readout period and preceding the next RF excitation. As well as applying the compensatory phase-encoding gradient, it is also necessary to have a constant net zero-order gradient moment sufficient to achieve resonance offset averaging (24).

For steady-state GRE imaging, it is well understood that spoiling or refocusing residual coherent transverse magnetization produces different steady-state magnetization values, leading to different image signal intensities and contrast (20, 22). Specifically, using the spoiled approach T_1 -dependent contrast is obtained (assuming a short echo time), and using the refocused approach contrast that depends on T_1 and T_2 is obtained. Also, signal levels are generally increased using the refocused approach. Furthermore, the differences between gradient spoiling and RF spoiling are well understood for steady-state GRE imaging. Using a straightforward gradient spoiling technique, the steady-state transverse magnetization closely approximates that calculated for ideal spoiling (transverse magnetization set equal to zero just before the next RF excitation) for many spatial positions; however, it differs significantly at some positions, which results in intensity banding artifacts in conventional magnitude reconstructed images (18–20). Using RF spoiling with the proper RF pulse phase-difference increment (e.g., 117°), the steady-state transverse magnetization closely approximates that for ideal spoiling for all spatial positions and is not position-dependent (18, 19).

For GRE imaging during the approach to steady state, it is generally understood that spoiling or refocusing the residual coherent transverse magnetization leads to fundamentally different approaches of the magnetization to steady state, and this affects image artifacts, signal inten-

MRM 35:237–245 (1996)

From the Departments of Radiology (F.H.E., J.P.M., J.R.B.) and Biomedical Engineering (J.P.M., J.R.B.), University of Virginia Health Sciences Center, Charlottesville, Virginia.

Address correspondence to: Frederick H. Epstein, PhD, W-827, GE Medical Systems, Waukesha, Wisconsin 53188.

Received March 1, 1995; revised August 23, 1995; accepted August 30, 1995.

This work was supported in part by a grant from the Whitaker Foundation and by Siemens Medical Systems.

Portions of this work were presented at the 1994 SMR meeting, Dallas, Texas.

0740-3194/96 \$3.00

Copyright © 1996 by Williams & Wilkins

All rights of reproduction in any form reserved.

sities, and contrast (13, 25, 26). However, to the best of our knowledge, a systematic analysis comparing the specific effects of each of the different methods of controlling residual transverse magnetization has not yet been presented. In this paper we present the results of a theoretical and experimental comparison of GRE imaging during the approach to steady state using gradient spoiling, RF spoiling, and gradient refocusing. By analyzing signal evolutions and corresponding images, we assess the impact of these different techniques on image artifacts and signal intensities. Finally, from our results, we develop suggestions for the appropriate use of each technique.

MATERIALS AND METHODS

Bloch Equation Simulation

The approach of the signal to steady state and corresponding simulated images of a phantom were calculated using a Bloch equation computer simulation of ideally spoiled, gradient-spoiled, gradient-refocused, and RF-spoiled short TR GRE imaging (this simulation program is based on the simulations of GRE imaging developed by Sekihara (20) and Zur *et al.* (19)). A pulse sequence diagram showing the different configurations of the short TR GRE pulse sequence is shown in Fig. 1. In the simulation program a series of one-dimensional data arrays is defined, one for each of the pertinent physical parameters of the object of interest, for which corresponding elements in the arrays define the parameter values for a specific point in the object. The parameter arrays include the components of the magnetization vector, the T_1 and T_2 relaxation times, the proton density, and the spatial

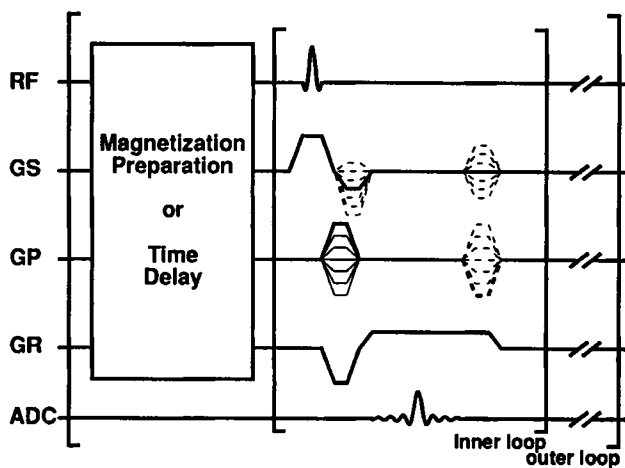


FIG. 1. Pulse sequence timing diagram for magnetization-prepared or segmented two-dimensional or three-dimensional short TR gradient-echo imaging. The gradient-refocused configuration includes the compensatory (second) gradient tables in the phase-encoding and section-select directions, whereas the gradient-spoiled configuration does not include these gradient tables. The RF-spoiled configuration is the same as the gradient-refocused configuration with the addition of a linear increase in the increment of the RF-pulse phase as the gradient-echo acquisition repeats. The outer loop is repeated for three-dimensional imaging, segmented two-dimensional imaging, or averaging.

position. A series of basic imaging operations is also defined, which operate on the magnetization vector given the corresponding parameter values. The imaging operations include RF pulses, gradient pulses, data sampling, and time delays. The RF pulses may be nonselective or section-selective. The gradient pulses may be applied along any of three orthogonal axes, and the pulse waveforms may have arbitrary shapes. Relaxation can occur during the gradient pulses, data sampling, and time delays. The simulation program was implemented in FORTRAN on a SPARCstation 10 computer (Sun Microsystems, Mountain View, CA).

Specifically, the simulation was conducted as follows for the short TR GRE pulse sequences. For all implementations of short TR GRE imaging, the RF and gradient waveforms and data sampling were applied as shown in Fig. 1, except, to shorten computational times, the RF pulse was usually modeled as nonselective (a few cases were simulated using both selective and nonselective RF excitations to evaluate the effects of assuming a nonselective RF excitation). For ideally spoiled short TR GRE, the transverse magnetization was set equal to zero immediately following each data sampling period. For gradient-spoiled, gradient-refocused, and RF-spoiled short TR GRE, the zero-order moment, $m_{0,R}$, of the readout gradient waveform over the TR was sufficiently large to achieve a uniform distribution of the transverse magnetization phase, $\phi_R(x_R)$ because of the gradient across each voxel in the readout direction. The zero-order moment and magnetization phase for a gradient applied in the i^{th} direction ($i = R$ [readout], P [phase encoding], or S [section select]) are given by

$$m_{0,i} = \int_0^{TR} G_i(t) dt \quad [1]$$

$$\phi_i(x_i) = \int_0^{TR} \omega(x_i, t) dt = \gamma x_i m_{0,i} \quad [2]$$

where t is time, $G_i(t)$ is the gradient waveform in the i^{th} direction, ω is frequency, x_i is distance along the i^{th} direction, and γ is the gyromagnetic ratio for protons. For gradient-refocused short TR GRE, the compensatory phase-encoding gradient was applied so that $m_{0,P}$ was zero. For gradient-spoiled short TR GRE, the compensatory phase-encoding gradient was not applied, resulting in an $m_{0,P}$ that varied with the GRE sequence repetition number and, furthermore, depended on the phase-encoding order. This nonzero variable $m_{0,P}$ caused $\phi_P(x_P)$ to vary in a manner dependent on the spatial position and the phase-encoding order. For RF-spoiled short TR GRE, the simulation was equivalent to that of gradient-refocused short TR GRE, except that the phase of the RF excitation pulse was incremented appropriately (19).

For all sequence configurations, the signal evolutions were calculated by performing a vector summation of the transverse magnetization across the readout direction (to be referred to as resonance offset averaging) at each spatial position (voxel center) in the phase-encoding direction. The simulated images depicted a square cross-section.

tion through a uniform phantom. The ratios of the phantom widths in the readout and phase-encoding directions to the respective fields of view (FOV) were 0.75. Also, noise was added to the simulated images to produce a signal-to-noise ratio of 100 for the brightest signal intensity. (With a noise level of zero, we found that minor signal intensity variations often appeared prominently in the simulated images, detracting from the major features of the images.)

Representative Cases

Using the Bloch equation simulation, representative cases for the different configurations of short TR GRE imaging were studied to characterize each configuration in terms of image artifacts and relative signal intensity. The following parameter values were chosen to be representative of MP-GRE imaging in the brain or abdomen (1, 27): $TR = 10$ ms; $TE = 5$ ms; flip angle (α) = 15° ; inversion time (TI) = 970 ms (assuming an inversion recovery magnetization preparation, this TI yields a normalized longitudinal magnetization value just before the short TR GRE acquisition, $M_z(TI)$, of 0.5 for $T_1 = 700$ ms); phase-encoding order equals sequential or centric; $T_1 = 700$ ms; and $T_2 = 110$ ms. These relaxation times were chosen to approximate at 1.5T those for several tissues of interest (e.g., brain matter, liver (28)) and to equal those for the phantom used for experimental confirmation of predictions generated by the simulation program. Simulated signal evolutions and corresponding images were generated using these parameter values for ideally spoiled, gradient-spoiled, gradient-refocused, and RF-spoiled (117° increment in the phase difference between successive RF pulses) MP-GRE.

The Bloch equation simulation was experimentally validated by acquiring corresponding images of a 150×150 mm agarose gel phantom with $T_1/T_2 = 700$ ms/110 ms using a 1.5T whole-body imager (Magnetom 63SP, Siemens Medical Systems, Iselin, NJ). Measurements were performed using a circularly polarized head coil or body coil, bandwidth = 217 Hz/pixel, FOV = 200 mm, section thickness = 10 mm, inter-shot delay = 2800 ms or 3500 ms, matrix = 128×128 , and 16 (head coil) or 124 (body coil) acquisitions for noise averaging. A large number of acquisitions was used to achieve a sufficient signal-to-noise ratio to resolve the detailed features of the image artifacts. The body coil was used in cases in which a uniform RF field was required to clearly illustrate the nature of the image artifacts.

Effects of Sequence Parameter Values on Image Artifacts

Each short TR GRE sequence configuration (e.g., gradient-spoiled and centric phase-encoding order) has a characteristic signal evolution behavior and corresponding image artifacts; however, the degree to which the non-uniform signal behavior adversely affects image appearance depends on the specific tissue relaxation times and sequence parameter values. Using the simulation program, we varied pulse sequence parameter values and tissue relaxation times to determine their effect on image appearance. Specifically, we considered parameter values in the ranges: $100 \text{ ms} \leq T_1 \leq 1000 \text{ ms}$, $50 \text{ ms} \leq T_2 \leq$

500 ms , $10^\circ < \alpha < 40^\circ$, $M_z(TI) = -0.5, 0.0, 0.5, \text{ or } 1.0$, phase-encoding order = sequential or centric, and control of transverse magnetization = gradient-spoiled, gradient-refocused, or RF-spoiled.

RF Spoiling during the Approach to Steady State

The RF-pulse phase-difference increment of 117° , which is commonly used for RF-spoiled steady-state GRE imaging, yields steady-state signal intensities that closely approximate those of ideally spoiled steady-state GRE imaging for a wide range of tissue relaxation times and excitation pulse flip angles (19). However, for GRE imaging during the approach to steady state, closely approximating the ideally spoiled GRE signal intensity once the measured signal has reached the steady state is not what is desired. A more appropriate goal is to closely approximate the transient signal evolution that would occur if the transverse magnetization for each excitation were ideally spoiled during the approach to steady state.

To optimize the RF-pulse phase-difference increment for RF spoiling during the approach to steady state, we simulated the signal amplitude and phase evolutions using RF-pulse phase-difference increments, ϕ , of -180° to 180° at 1° intervals for a range of sequence parameters and tissue relaxation times and calculated the sums of squared differences of both the amplitude ($\sum_{(\Delta A)}^2(\phi)$) and phase ($\sum_{(\Delta \Phi)}^2(\phi)$) evolutions from the corresponding ideally spoiled evolutions. The following T_1/T_2 relaxation time combinations were used: 100 ms/100 ms, 1000 ms/100 ms, 1000 ms/200 ms, and 1000 ms/500 ms; the following sequence parameter values were used: $M_z(TI) = -0.5$ or 0.5 and $\alpha = 10^\circ, 20^\circ, 30^\circ$. The goal was to either find an RF-pulse phase-difference increment, ϕ' , which minimized $\sum_{(\Delta A)}^2(\phi)$ and $\sum_{(\Delta \Phi)}^2(\phi)$ for all cases or which satisfied $\sum_{(\Delta A)}^2(\phi) < \sum_{(\Delta A)}^2(\phi = 117^\circ)$ and $\sum_{(\Delta \Phi)}^2(\phi) < \sum_{(\Delta \Phi)}^2(\phi = 117^\circ)$ for all or the majority of the cases considered.

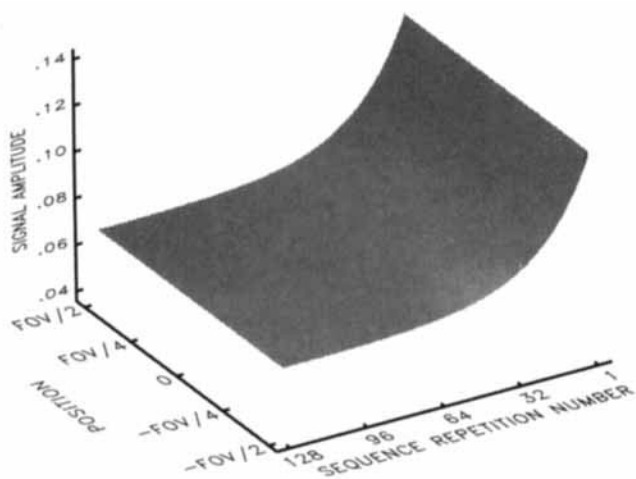
Clinical Imaging Example

As a clinical imaging example, after informed consent was obtained, we imaged liver transplant patients with ascites using gradient-spoiled, gradient-refocused, and RF-spoiled MP-GRE and the sequential phase-encoding order. Because ascites is a peritoneal accumulation of fluid, it has a relatively long T_2 and is known to conspicuously show image artifacts related to the method used for controlling the transverse magnetization.

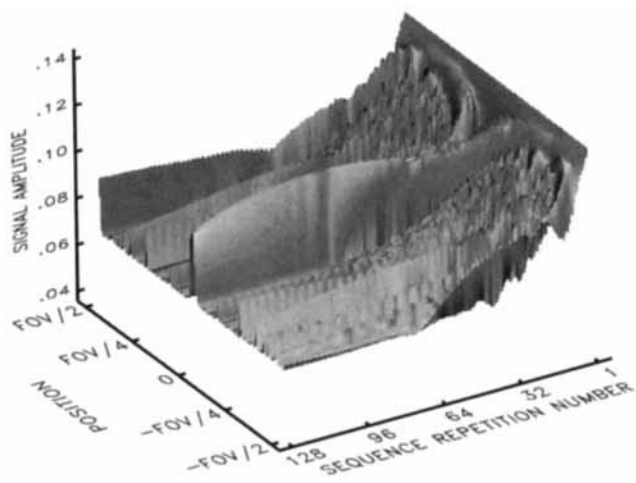
RESULTS

Representative Cases

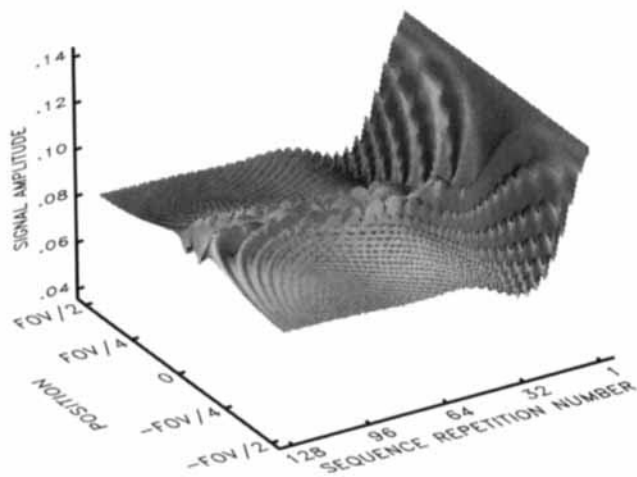
In Fig. 2, simulated signal amplitude evolutions for (a) ideally spoiled MP-GRE, (b) gradient-spoiled MP-GRE with sequential phase-encoding, (c) gradient-spoiled MP-GRE with centric phase-encoding, (d) gradient-refocused MP-GRE, and (e) RF-spoiled (RF-pulse phase-difference increment = 117°) MP-GRE are shown as a function of the position along the phase-encoding direction and the GRE sequence repetition number. The relaxation times and parameter values for Fig. 2 are as given in the Mate-



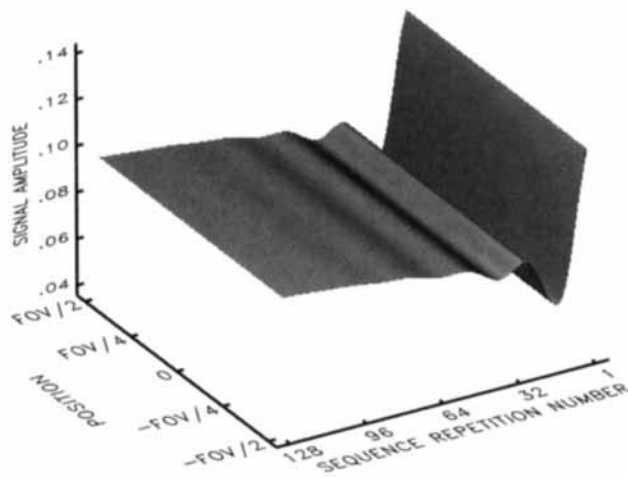
a



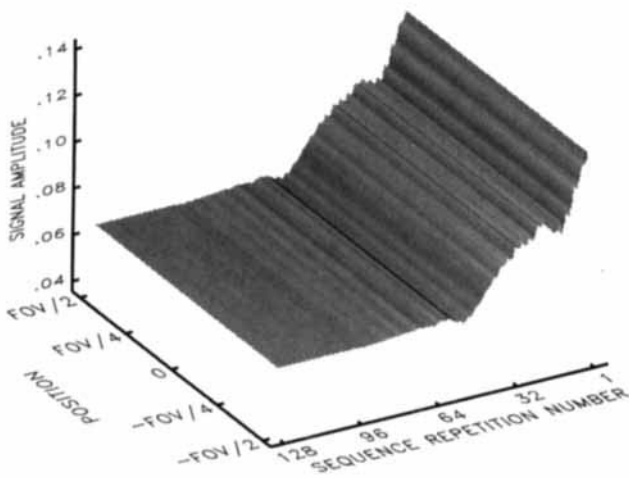
b



c



d



e

FIG. 2. Simulated signal amplitude evolutions, as a function of the position along the phase-encoding direction and the GRE sequence repetition number, for representative MP-GRE imaging using (a) ideal spoiling, (b) gradient spoiling and sequential phase encoding, (c) gradient spoiling and centric phase encoding, (d) gradient refocusing, and (e) RF spoiling (RF-pulse phase-difference increment = 117°). Parameters for these simulations were $TR = 10$ ms, $TE = 5$ ms, $\alpha = 15^\circ$, $M_z(TI) = 0.5$, and $T_1/T_2 = 700$ ms/110 ms.

rials and Methods section. For the case of ideally spoiled MP-GRE, the signal evolution is not position-dependent and is monotonically decreasing. For gradient-spoiled MP-GRE with sequential phase-encoding, the signal evo-

lution closely approximates that of ideally spoiled MP-GRE for some spatial positions; however, at other positions it deviates substantially from the ideally spoiled case. For gradient-spoiled MP-GRE with centric phase-

encoding, the signal initially drops off rapidly, and then oscillates toward the steady state, with oscillatory behavior being more pronounced toward the center of the FOV (position = 0). Case (c) is markedly different than case (b), clearly demonstrating the impact of phase-encoding order on the signal evolution when using gradient spoiling. For gradient-refocused MP-GRE, we obtained the familiar result that initially the signal drops off rapidly, oscillates toward the steady state, and is not position-dependent. Finally, for RF-spoiled MP-GRE the signal amplitude evolution generally approximates that of ideally spoiled MP-GRE at all spatial positions, is not dependent on position, and displays relatively small jagged changes with the GRE sequence repetition number.

Figure 3 shows simulated images generated using both the sequential and centric phase-encoding orders for all signal evolutions of Fig. 2. For ideally spoiled MP-GRE, relatively artifact free images are obtained using both sequential (Fig. 3a) and centric (Fig. 3b) phase-encoding orders. For gradient-spoiled MP-GRE with sequential phase encoding (Fig. 3c), intensity banding artifacts are clearly seen. The positions of the intensity bands are the same as those described previously for steady-state GRE imaging (18–20). For gradient-spoiled MP-GRE with centric phase encoding (Fig. 3d), a wide hypointense band bordered by hyperintense bands is observed at the center of the image, and relatively homogeneous signal intensity is achieved laterally. Also, loss of edge definition because of the low pass filter effects of the signal evolution can be seen. For gradient-refocused MP-GRE with sequential phase encoding (Fig. 3e), a relatively artifact-free image is observed; however, the signal intensity is increased compared with ideally spoiled MP-GRE. With more than one tissue, this effect could lead to image contrast that is different than the spoiled case. For gradient-refocused MP-GRE with centric phase encoding (Fig. 3f), loss of edge definition is prominent, again corresponding to the low pass filter effect. Finally, for RF-spoiled MP-GRE, relatively artifact-free images are ob-

tained using both sequential (Fig. 3g) and centric (Fig. 3h) phase-encoding orders. With centric phase encoding, some loss of edge definition is evident; however, it is less than for the gradient-refocused case.

For the simulated images that were calculated using both selective and nonselective RF pulses, we found that, although the quantitative signal intensities at some locations in the images were substantially different, the overall image appearance (general artifact pattern) was very similar. For this reason, we felt that simulations using nonselective excitation were sufficient to assess the general image properties for both selective and nonselective RF pulses. Note that the simulated images in Figs. 3 and 5 (nonselective excitation) compare favorably with their experimental counterparts in Figs. 4 and 6 (two-dimensional selective excitation). The simulated images using nonselective excitation could be calculated in at most a few hours of computer time per case, compared with a maximum of more than a day of computer time per case for selective excitation.

Images of the agarose gel phantom corresponding to the simulated images of Fig. 3, c–h, are shown in Fig. 4. Excellent agreement between measured image appearance and simulated image appearance is seen for all sequence configurations.

Effects of Sequence Parameter Values on Image Artifacts

For gradient-spoiled MP-GRE using both the sequential and centric phase-encoding orders, intensity banding artifacts similar to those shown in Fig. 2 were subtly apparent using low flip angles (e.g., 10°) and short relaxation times (e.g., 50 ms) and became more prominent as the flip angle and/or T_2 increased. The general appearance of the artifacts was found to be largely independent of T_1 and $M_z(TI)$. Similarly, for gradient-refocused MP-GRE and sequential phase encoding, the change in image signal intensity and contrast from those of ideally spoiled MP-GRE increased as flip angle and/or T_2 increased, and, using centric phase encoding, image blurring increased under these conditions.

For RF-spoiled MP-GRE, the jaggedness of the signal evolution (see Fig. 2e) became more pronounced as flip angle and/or T_2 increased. Simulated images demonstrat-

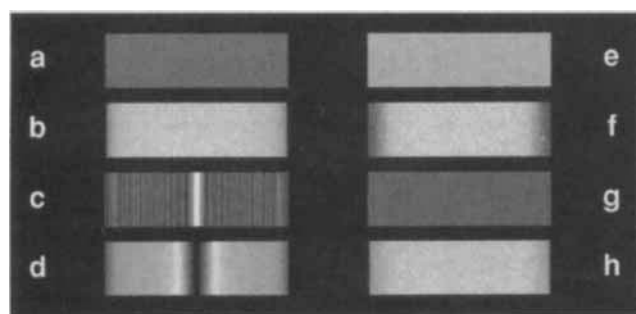


FIG. 3. Simulated images of a uniform phantom generated using all combinations of sequential and centric phase encoding and the signal evolutions of Fig. 2. (a) Ideal spoiling and sequential phase encoding. (b) Ideal spoiling and centric phase encoding. (c) Gradient spoiling and sequential phase encoding. (d) Gradient spoiling and centric phase encoding. (e) Gradient refocusing and sequential phase encoding. (f) Gradient refocusing and centric phase encoding. (g) RF spoiling and sequential phase encoding. (h) RF spoiling and centric phase encoding. (The original images have been cropped along the readout direction to provide a more compact presentation. The displayed images are 28×128 pixels.)

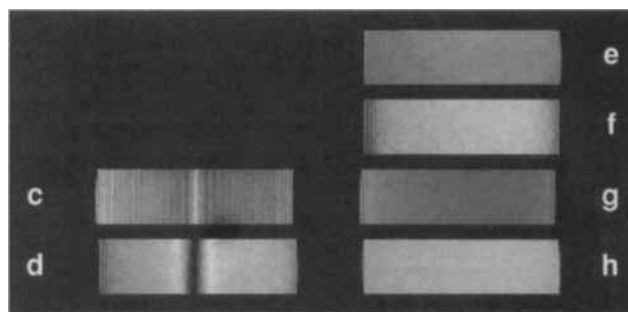


FIG. 4. Measured images of an agarose gel phantom with $T_1/T_2 = 700$ ms/110 ms. These images correspond to the simulated images of Fig. 3 and are arranged in the same order. Images (a) and (b) are blank because there is no experimental case corresponding to ideal spoiling. (The original images have been cropped along the readout direction to provide a more compact presentation. The displayed images are 28×128 pixels.)

ing the effects of this signal behavior, showing intensity banding artifacts (sequential phase encoding) and image blurring (centric phase encoding) are shown in Fig. 5 for $T_1/T_2 = 700$ ms/110 ms, $M_z(TI) = 0.5$, $\alpha = 10^\circ, 20^\circ, 30^\circ$, or 40° , and phase-encoding order equals sequential and centric. For RF spoiling and sequential phase encoding, the banding artifacts in measured images were well visualized only for $\alpha = 40^\circ$ (see Fig. 6).

Optimization of RF Spoiling during the Approach to Steady State

Two important results were obtained from the study of the approach of the signal to steady state for RF-spoiled MP-GRE using different RF-pulse phase-difference increments. First, we found that no single value of the RF-pulse phase-difference increment, φ , minimized $\Sigma_{(\Delta A)^2}(\varphi)$ and $\Sigma_{(\Delta \Phi)^2}(\varphi)$ for all of the relaxation time, sequence parameter value combinations considered. However, we did find that $\varphi = 84^\circ$ satisfied $\Sigma_{(\Delta A)^2}(\varphi = 84^\circ) < \Sigma_{(\Delta A)^2}(\varphi = 117^\circ)$ and $\Sigma_{(\Delta \Phi)^2}(\varphi = 84^\circ) < \Sigma_{(\Delta \Phi)^2}(\varphi = 117^\circ)$ for most cases. As an example, Fig. 7 shows the signal amplitude and phase evolutions for one case using ideal spoiling, RF spoiling with $\varphi = 117^\circ$, and RF spoiling with $\varphi = 84^\circ$. (We did not perform an experimental comparison of $\varphi = 84^\circ$ and $\varphi = 117^\circ$ because the $\varphi = 84^\circ$ cannot currently be implemented on our imager.)

Second, we found that each RF-pulse phase-difference increment value corresponds to one spatial position using gradient spoiling and sequential phase encoding. Figure 8 shows the signal amplitude evolutions for RF-spoiled MP-GRE imaging with $T_1/T_2 = 700$ ms/110 ms and RF-pulse phase-difference increments of -180° to 180° at 1° intervals. Comparing Fig. 8 with Fig. 2b, we see that they are identical. This indicates that for RF-spoiled MP-GRE, the signal evolution for any given RF-pulse phase-difference increment corresponds to the signal evolution at one spatial location along the phase-encoding direction using gradient-spoiled MP-GRE with sequential phase encoding. In these calculations, the signal is the integral of the transverse magnetization over a

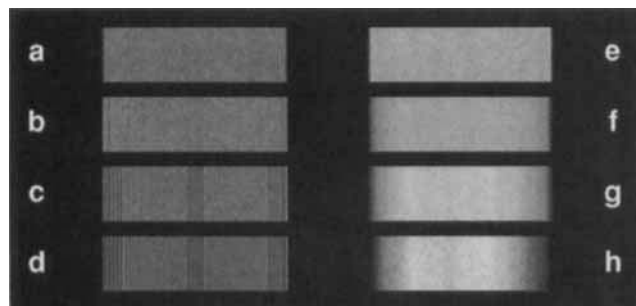


FIG. 5. Simulated images of a uniform phantom generated using RF spoiling and sequential phase encoding with (a) $\alpha = 10^\circ$, (b) $\alpha = 20^\circ$, (c) $\alpha = 30^\circ$, and (d) $\alpha = 40^\circ$ and using centric phase encoding with (e) $\alpha = 10^\circ$, (f) $\alpha = 20^\circ$, (g) $\alpha = 30^\circ$, and (h) $\alpha = 40^\circ$. Other parameters for these simulations were $TR = 10$ ms, $TE = 5$ ms, $M_z(TI) = 0.5$, $T_1/T_2 = 700$ ms/110 ms, and RF-pulse phase-difference increment = 117° . (The original images have been cropped along the readout direction to provide a more compact presentation. The displayed images are 28×128 pixels.)

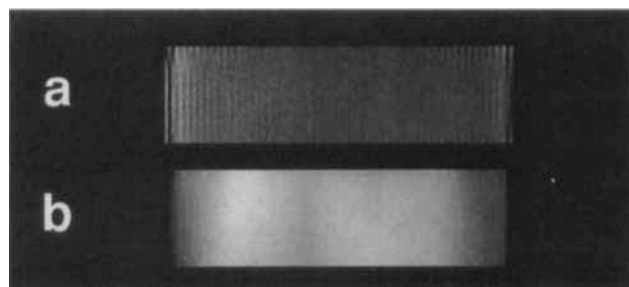


FIG. 6. (a), (b) Measured images of an agarose gel phantom with $T_1/T_2 = 700$ ms/110 ms corresponding to the simulated images (d) and (h), respectively, of Fig. 5. (The original images have been cropped along the readout direction to provide a more compact presentation. The displayed images are 28×128 pixels.)

uniform distribution of resonance offsets in the readout direction.

Clinical Imaging Examples

Images of a patient with ascites acquired with (a) gradient-spoiled, (b) gradient-refocused, and (c) RF-spoiled MP-GRE, each using sequential phase encoding and $\alpha = 10^\circ$, are shown in Fig. 9. Intensity bands can be seen using gradient spoiling, and altered image contrast (particularly in the ascites) is seen with gradient refocusing. Using RF spoiling, artifact-free images that maintain the original image contrast are achieved.

CONCLUSIONS AND DISCUSSION

GRE imaging during the approach to steady state is routinely used for numerous MR imaging applications and is being evaluated for more. Image artifacts, signal intensity, and contrast for this pulse sequence are largely determined by whether the residual transverse magnetization is spoiled or refocused, and, if spoiled, the spoiling method used. We used a Bloch equation simulation and experimental methods to study multiple configurations of this pulse sequence, specifically considering different methods of spoiling or refocusing the residual transverse magnetization. The different methods included gradient spoiling, gradient refocusing, and RF spoiling. For each method, a characteristic signal evolution behavior and corresponding image appearance was demonstrated, and the effects of changing sequence parameter values were investigated. Also, the RF-pulse phase-difference increment used for RF spoiling was optimized for imaging during the approach to steady state.

For the gradient-spoiled configuration, or any configuration where $m_{0,p}$ varies with sequence repetition, the signal will evolve differently at different spatial positions in the phase-encoding direction. In this situation, image artifacts arise from two sources. One source is the dependence on spatial position of the signal evolution. This leads to intensity banding. A second source is the non-uniformity of the signal evolutions. This results in degraded point spread functions and corresponding image artifacts such as blurring or ghosting. For example, Figs. 3d and 4d show both intensity banding and loss of edge definition. Furthermore, when the variability of $m_{0,p}$ decreases

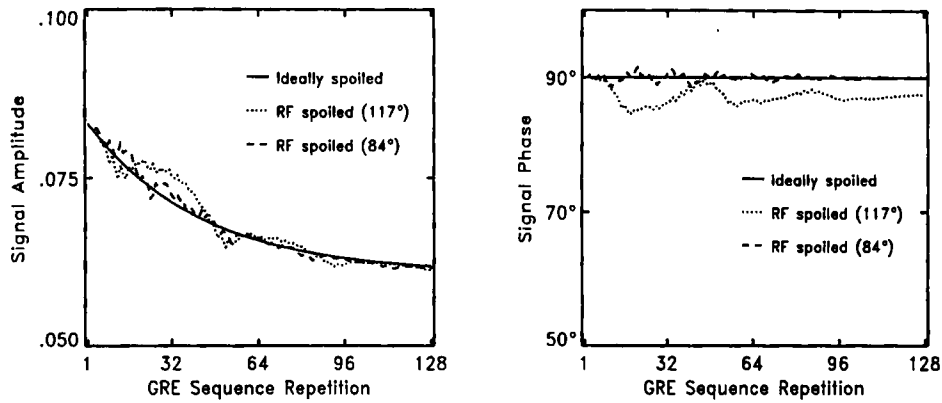


FIG. 7. Signal amplitude and phase evolutions for ideally spoiled, RF-spoiled (RF-pulse phase-difference increment = 117°), and RF-spoiled (RF-pulse phase-difference increment = 84°) MP-GRE imaging with $M_z(TI) = 0.5$, $\alpha = 10^\circ$, $TR = 10$ ms, $TE = 5$ ms, and relaxation times of $T_1 = 1000$ ms and $T_2 = 100$ ms. In this example of RF-spoiled MP-GRE imaging, an RF-pulse phase-difference increment of 84° provides a closer approximation to the ideally spoiled MP-GRE signal amplitude and phase evolutions than an RF-pulse phase-difference increment of 117°.

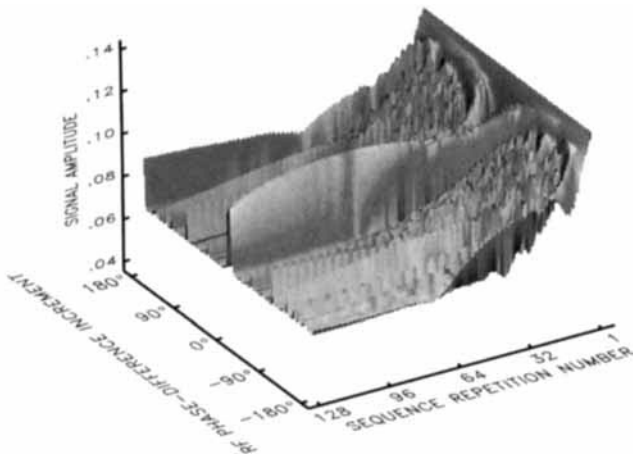


FIG. 8. Simulated signal amplitude evolution, as a function of the RF-pulse phase-difference increment and the GRE sequence repetition number, for RF-spoiled MP-GRE imaging with $TR = 10$ ms, $TE = 5$ ms, $\alpha = 15^\circ$, $M_z(TI) = 0.5$, and $T_1/T_2 = 700$ ms/110 ms. This plot is identical to Fig. 2b, which shows the signal amplitude evolution for gradient-spoiled MP-GRE using sequential phase encoding as a function of the position along the phase-encoding direction and the GRE sequence repetition number.

depends on the phase-encoding order, the signal evolution also depends on the phase-encoding order, as demonstrated in Fig. 2, b and c.

The primary advantage of using gradient spoiling is that the compensatory phase-encoding gradient(s) need not be applied, thereby allowing for a shorter TR . Achieving the shortest possible TR can sometimes be an important requirement (e.g., see Ref. 29), and in this case using gradient spoiling in conjunction with a flip angle of approximately 10° or less may be appropriate. With higher flip angles (approximately 15° or greater) or long T_2 values (approximately 200 ms or greater) intensity banding artifacts become very apparent. Also, more sophisticated implementations of gradient spoiling are possible when gradient pulses are applied after the data readout period (17). However, with this approach the TR is substantially increased, and it is still difficult to en-

tirely eliminate the spatial dependence of the signal evolution.

For the gradient-refocused configuration, the signal is independent of position and phase-encoding order, oscillates toward the steady state, and does not closely approximate the ideally spoiled signal evolution, particularly at flip angle values above approximately 15°. Using the sequential phase-encoding order, the signal amplitude oscillations occur primarily at high spatial frequencies and may not cause noticeable image artifacts. However, the resulting signal intensity at low spatial frequencies will be weighted by both the tissue T_1 and T_2 and, therefore, may not produce the desired image contrast. Using the centric phase-encoding order, the oscillatory signal behavior occurs at low spatial frequencies and causes loss of edge definition. The blurring can be reduced by discarding the initial data acquisitions; however, this is generally accompanied by a loss in image signal intensity and contrast. Implementations using relatively high flip angles (e.g., 30°), discarded data acquisitions, and the centric phase-encoding order have been used successfully for liver imaging (1). A comparison of this technique with an RF-spoiled sequence using a flip angle of approximately 15–20° would be interesting. An alternative approach for the gradient-refocused sequence, which has been previously investigated in some detail, is the use of flip angles which vary as a function of the GRE sequence repetition number to specifically shape the signal evolution (30, 31).

For the RF-spoiled configuration, the signal is independent of position and phase-encoding order, and, for T_2 values of less than approximately 200 ms, closely approximates the ideally spoiled signal evolution using flip angles below approximately 20°. Nonideal behavior of the signal is manifested as unsmooth variations in the signal amplitude and phase evolutions as the GRE sequence repeats. With sequential phase encoding, this signal behavior was shown to produce PSF-induced banding artifacts in a uniform phantom, which become prominent at flip angles above approximately 20°. With centric phase encoding, significant image blurring occurred under these conditions. However, using flip an-



FIG. 9. MP-GRE images of a patient with ascites using sequential phase encoding, $\alpha = 10^\circ$, and (a) gradient spoiling, (b) gradient refocusing, and (c) RF spoiling (RF-pulse phase-difference increment = 117°).

gles of less than approximately 20° and T_2 values of less than approximately 200 ms, image artifacts were minimal.

We also investigated improving RF spoiling specifically for imaging during the approach to steady state. We found that using RF-pulse phase-difference increments other than 117° , such as 84° , it is possible to more closely approximate the ideally spoiled signal amplitude and phase evolution over the range of relaxation times and sequence parameters considered. Also, it is possible that varying the RF-pulse phase difference in ways other than a linear increment may achieve more complete spoiling during the approach to steady state. This possibility should be investigated in the future.

A further finding was that each RF-pulse phase-difference increment produces a signal evolution that corresponds to one spatial position using gradient spoiling and sequential phase encoding. This result was obtained because the signal was calculated using resonance offset averaging. The same result does not hold for individual magnetization vectors, because the effect of applying an RF pulse with a given phase to a single magnetization vector is not identical to applying a gradient that imparts that same phase to the transverse component of the magnetization vector. However, when averaged over resonance offsets, the same result is achieved. Additionally, we found that using RF spoiling without applying the compensatory phase-encoding gradient(s) results in intensity banding artifacts that are altered compared with the gradient-spoiled case, but not eliminated. The intensity banding artifacts are still present because they come from the gradient-induced position-dependent accumulation of phase, which occurs using this configuration.

In conclusion, we found that, under a fairly wide range of clinically relevant conditions, RF spoiling is an effective and spatially consistent way to closely approximate the ideally spoiled approach to steady state of the measured signal. Although RF spoiling during the approach to steady state does not provide the nearly exact approximation to ideal spoiling as that attained for steady-state GRE, by using the proper RF-pulse phase-difference increment, it is clearly superior to gradient spoiling. It is also important to realize that, although RF spoiling in steady-state GRE is effective for a wide range of flip angles and relaxation times, for RF spoiling during the approach to steady state jagged variations in the signal

evolution and associated image artifacts are seen when using high flip angles and/or long T_2 values.

ACKNOWLEDGMENTS

The authors thank Eduard E. de Lange, MD, for many helpful discussions regarding the clinical goals of abdominal MRI.

REFERENCES

1. A. F. Holsinger-Bampton, S. J. Riederer, N. G. Campeau, R. L. Ehman, C. D. Johnson, T1-weighted snapshot gradient-echo MR imaging of the abdomen. *Radiology* **181**, 25–32 (1991).
2. E. E. de Lange, J. P. Mugler III, J. E. Bosworth, G. A. DeAngelis, S. B. Gay, N. S. Hurt, S. S. Berr, J. M. Rosenblatt, L. W. Merickel, E. K. Harris, MR imaging of the liver: breath-hold T1-weighted MP-GRE compared with conventional T2-weighted SE imaging—lesion detection, localization, and characterization. *Radiology* **190**, 727–736 (1994).
3. M. Brant-Zawadzki, G. D. Gillan, W. R. Nitz, MP-RAGE: a three-dimensional, T1-weighted, gradient-echo sequence—initial experience in the brain. *Radiology* **182**, 769–775 (1992).
4. T. K. F. Foo, A. M. Sawyer, W. H. Faulkner, D. G. Mills, Inversion in the steady state: contrast optimization and reduced imaging time with fast three-dimensional inversion-recovery—prepared GRE pulse sequences. *Radiology* **191**, 85–90 (1994).
5. J. S. Ross, J. A. Tkach, J. Dillinger, P. M. Ruggieri, T. J. Masaryk, M. T. Modic, Optimization of three-dimensional T1-weighted gradient-echo imaging of the cervical spine. *J. Magn. Reson. Imaging* **2**, 359–364 (1992).
6. D. J. Atkinson, R. R. Edelman, Cineangiography of the heart in a single breath hold with a segmented TurboFLASH sequence. *Radiology* **178**, 357–360 (1991).
7. J. Frahm, K. D. Merboldt, M. L. Gyngell, W. Hanicke, D. Chien, 0.3-second FLASH MRI of the human heart. *Magn. Reson. Med.* **13**, 150–157 (1990).
8. D. Li, C. B. Paschal, E. M. Haacke, L. P. Adler, Coronary arteries: three-dimensional MR imaging with fat saturation and magnetization transfer contrast. *Radiology* **187**, 401–406 (1993).
9. R. R. Edelman, W. J. Manning, D. Burstein, S. Paulin, Coronary arteries: breath-hold MR angiography. *Radiology* **181**, 641–643 (1991).
10. D. Li, E. M. Haacke, J. P. Mugler III, S. Berr, J. R. Brookeman, M. C. Hutton, Three-dimensional time-of-flight MR angiography using selective inversion recovery RAGE with fat

- saturation and ECG-triggering: application to renal arteries. *Magn. Reson. Med.* **31**, 414–422 (1994).
11. A. Haase, D. Matthaei, R. Bartkowski, E. Duhmke, D. Leibfritz, Inversion recovery snapshot FLASH MR imaging. *J. Comput. Assist. Tomogr.* **13**, 1036–1040 (1989).
 12. W. Hanicke, K. D. Merboldt, D. Chien, M. L. Gyngell, H. Bruhn, J. Frahm, Signal strength in sub-second FLASH magnetic resonance imaging: the dynamic approach to steady state. *Med. Phys.* **17**, 1004–1010 (1990).
 13. R. A. Jones, P. A. Rinck, Approach to equilibrium in snapshot imaging. *Magn. Reson. Imaging* **8**, 797–803 (1990).
 14. J. Frahm, W. Hanicke, K. D. Merboldt, Transverse coherence in rapid FLASH NMR imaging. *J. Magn. Reson.* **72**, 307–314 (1987).
 15. M. L. Wood, V. M. Runge, Artifacts due to residual magnetization in three-dimensional magnetic resonance imaging. *Med. Phys.* **15**, 825–831 (1988).
 16. M. L. Wood, M. Silver, V. M. Runge, Optimization of spoiler gradients in FLASH MRI. *Magn. Reson. Imaging* **5**, 455–463 (1987).
 17. H. Z. Wang, S. J. Riederer, A spoiling sequence for suppression of residual transverse magnetization. *Magn. Reson. Med.* **15**, 175–191 (1990).
 18. A. P. Crawley, M. I. Wood, R. M. Henkelman, Elimination of transverse coherences in FLASH MRI. *Magn. Reson. Med.* **8**, 248–260 (1988).
 19. Y. Zur, M. L. Wood, I. J. Neuringer, Spoiling of transverse magnetization in steady-state sequences. *Magn. Reson. Med.* **21**, 251–263 (1991).
 20. K. Sekihara, Steady-state magnetizations in rapid NMR imaging using small flip angles and short repetition intervals. *IEEE Trans. Med. Imaging* **MI-6** 157–164 (1987).
 21. Y. Zur, S. Stokar, P. Bendel, An analysis of fast imaging sequences with steady-state transverse magnetization refocusing. *Magn. Reson. Med.* **6**, 175–193 (1988).
 22. P. van der Meulen, J. P. Groen, A. M. C. Tinus, G. Bruntink, Fast Field Echo Imaging: An Overview and Contrast Calculations. *Magn. Reson. Imaging* **6**, 355–368 (1988).
 23. M. L. Gyngell, The application of steady-state free precession in rapid 2DFT NMR imaging: FAST and CE-FAST sequences. *Magn. Reson. Imaging* **6**, 415–419 (1988).
 24. E. M. Haacke, J. A. Tkach, Fast MR imaging: techniques and clinical applications. *AJR* **155**, 951–964 (1990).
 25. D. Chien, D. J. Atkinson, R. R. Edelman, Strategies to improve contrast in TurboFLASH imaging: reordered phase encoding and K-Space segmentation. *J. Magn. Reson. Imaging* **1**, 63–70 (1991).
 26. S. B. Reeder, E. R. McVeigh, Tag contrast in breath-hold CINE cardiac MRI. *Magn. Reson. Med.* **31**, 521–525 (1994).
 27. E. E. de Lange, J. P. Mugler III, J. A. Bertolina, et al. Magnetization-prepared Rapid Gradient-Echo (MP-RAGE) MR imaging of the liver: comparison with spin-echo imaging. *Magn. Reson. Imaging* **9**, 469–476 (1991).
 28. P. A. Bottomley, C. J. Hardy, R. E. Argersinger, G. Allen-Moore, A review of ¹H nuclear magnetic resonance relaxation in pathology: are T1 and T2 diagnostic? *Med. Phys.* **14**, 1–37 (1987).
 29. T. A. Tasciyan, D. G. Mitchell, Pulsatile flow artifacts in fast magnetization-prepared sequences. *J. Magn. Reson. Imaging* **4**, 217–222 (1994).
 30. J. P. Mugler III, F. H. Epstein, J. R. Brookeman, Shaping the signal response during the approach to steady state in three-dimensional magnetization-prepared rapid gradient-echo imaging using variable flip angles. *Magn. Reson. Med.* **28**, 165–185 (1992).
 31. F. H. Epstein, J. P. Mugler III, J. R. Brookeman, Improved T1-weighted two-dimensional MP-GRE imaging of the liver with variable flip angles for shaping the signal evolution. *J. Magn. Reson. Imaging* **4**, 91–98 (1994).